Special Issue: Prevention and control of COVID-19 transmission in the indoor environment

Indoor and Built Environment

Indoor and Built Environment
2022, Vol. 31(5) 1242–1261

DOI: 10.1177/1420326X211039546
journals.sagepub.com/home/ibe
SAGE

Simulation of COVID-19 indoor emissions from coughing and breathing with air conditioning and mask protection effects

Carlo Cravero and Davide Marsano

Abstract

The COVID-19 infection has emerged as a disruptive pandemic at worldwide level. The study of the mechanism of contagion is one of the greatest challenges before a mass vaccination campaign that would protect populations. The study can support the development of knowledge and tools to develop possible strategies for containing its spread in future events. The saliva droplet aerosol expelled during breathing or coughing is the main cause for the propagation of the SARS-Cov-2. In this work, a URANS CFD approach was used to simulate the dispersion from the mouth of these particles in closed environments. The air conditioning system was considered. The conditions were varied to determine their impact on the diffusion of the aerosol. Lagrangian and Eulerian numerical approaches were used to model the coughing and the breathing events. These were validated with the puff theory, numerical and experimental results. A realistic case of a meeting room with two persons was simulated. Different characteristics of the expulsed aerosols and different ventilation system configurations were considered to demonstrate how these simulations can support management strategies for indoor occupation. Finally, the effect of the protective mask was introduced to quantify its beneficial effects to support safe indoor occupation.

Keywords

CFD, SARS-Cov-2, COVID-19 infection, Saliva aerosol, Indoor safety, HVAC, Coughing and breathing

Accepted: 28 July 2021

Introduction

The global emergency resulting from the current COVID-19 pandemic has led the entire scientific community to commit its efforts to the various problems concerning the spread of the SARS-CoV-2 virus. In particular, its high contagiousness has alerted scientists to focusx on the main work to understand what exactly the mechanism of this contagion as. This pathogen of the coronavirus group can be assumed as almost spherical particle of 0.125 (0.05–0.2) μm in diameter.[1] The World Health Organization has established that it is transmitted from person to person mainly by the saliva particles emitted following a cough or sneeze, trough contact with oral, nasal and ocular mucous membranes.[2] Moreover, numerous studies link virus transmission to the formation of aerosols and droplets with a size of 5–10 μm even during breathing or common speech. The dispersion from this last phenomenon is related to the volume of vocalization. Depending on the particle size, they can travel different distances, while the air residence period can be prolonged for smaller particles. In an indoor environment,

Dipartimento di Ingegneria Meccanica, Energetica, Gestionale e dei Trasporti (DIME), University of Genoa, Genoa, Italy

Corresponding author:
Davide Marsano, Università degli Studi di Genoa, Via Montallegro 1, Genoa 16126, Italy.
Email: davide.marsano@edu.unige.it

the ventilation or air conditioning systems can play a crucial role in contaminant diffusion and dispersion.

The recent epidemics of the early 2000s, concerning SARS, swine flu and MERS have already produced some experimental and numerical evidence published in literature, especially in the most affected countries (East), to model the spread of the respective pathogen. A significant number of investigations are focused on different aspects of normal breathing and coughing. Basic or more realistic geometries of the airways for the simulation of airflow have been introduced to study the droplets formation.[3–6] Zhu et al.[7] measured the maximum speed of the air that leaves the mouth during a cough. Malve et al.[8] and Rahiminejad et al.[9] predicted numerically the velocity profile in the trachea during a cough event. Moreover, various researchers focused on the size of droplets of coughs and sneeze through experimental measures.[10–13] However, a recent work[14] measuring Influenza virus presence in droplets from a coughing patient noted that the Influenza virus was present in more than 60% for droplets/particles sized under 5 μm, making the smaller particles the most interesting ones to analyse. The fluid dynamic characteristics of coughs and sneezes have been investigated in literature and a series of experimental measurements focused on the maximum massflow rate.[15–17] The modelling of the droplets dispersion released by breathing in closed environments with heating, ventilating and air-conditioning (HVAC) system has been also investigated.[18–24] The fluid dynamic model can be integrated with a probabilistic approach to estimate the risk of an infection in an indoor ambient or to estimate the relative pathogens quantity in the contact surface on hands.[25–29] For this reason, a fluid-dynamic model to predict the detailed evolution of the dispersion of droplet particles from respiratory events in a closed environment is very crucial.

Some recent works on the COVID pandemic[30] have been verified through direct numerical simulations (DNS) that the claimed interpersonal distance of 1 m cannot guarantee the avoidance of the pathogen virus transmission. They have calculated the puff evolution with different particle diameters distribution in calm ambient. However, in the everyday life, it is very important to consider the respiratory phenomena in the actual indoor contest to be able to get realistic results from simulations in order to develop protection strategies for occupants and for the safe use of the indoor ambient. With this in mind, an Unsteady Reynolds-Averaged Navier-Stokes (URANS) computational fluid dynamics (CFD) approach has been setup to characterize the aerosol particles dispersions and water vapour during the breathing, coughing or sneezing, in order to simulate the evolution of saliva (droplets or aerosol) in indoor environments and to predict the effects of air conditioning systems and protective face masks. The experience gained by the research group in the field of industrial and environmental fluid dynamics[31–34] has allowed the use of these versatile and very robust CFD models. The respiratory puff evolution theory and experimental data have been used for the validation of these models for the coughing event case. A different numerical model from literature has then been used for the validation in the normal breathing case.

In our study, two different numerical approaches were considered and developed. One was used to study the evolution of a water particles population (with a prescribed size distribution) released into an enclosed environment by a person (Lagrangian approach). Another is a more representative of the water vapour formation and aerosols evolution from the dispersion phases to the environment by the occupant (Eulerian approach). Two cases were considered: an empty confined room or a confined room with occupants. In the latter case, different air conditioning settings were considered. Finally, the effect of the protective devices (masks) adopted by indoor occupants was modelled to compare different situations in order to support the management strategies of the ambient. The main target of the paper is to provide a model capable of giving a scientific support to the management of the health crisis by simulating situations of possible contagion due to the release of saliva particles in enclosed environments.

Mathematical model

Puff model

To validate the CFD model, the puff model proposed by Balachandar et al.[35] and the experimental work of Liu and Novoselac[36] have been used. The puff model pursued to obtain a simple solution of the temporal evolution of the puff from exhalation. The dimensionless axial distance from the injection source to the jet tip can be calculated by varying some puff quantities. This theory starts from horizontal and vertical momentum balances, which are reported in non-dimensional form as described by equations (1) and (2)

$$\frac{d}{d\tilde{t}}\left[\left(r_m\frac{d\tilde{s}}{d\tilde{t}}+\frac{1}{4}\frac{d\tilde{s}^4}{d\tilde{t}}\right)\cos\theta\right]=-C\tilde{s}^2\left(\frac{d\tilde{s}}{d\tilde{t}}\right)^2\cos\theta \quad (1)$$

$$\frac{d}{d\tilde{t}}\left[\left(r_m\frac{d\tilde{s}}{d\tilde{t}}+\frac{1}{4}\frac{d\tilde{s}^4}{d\tilde{t}}\right)\sin\theta\right]=A-C\tilde{s}^2\left(\frac{d\tilde{s}}{d\tilde{t}}\right)^2\sin\theta \quad (2)$$

where the non-dimensional axial distance and time are calculated, as the distance travelled from the virtual

origin at the corresponding time, as reported in equations (3) and (4)

$$\tilde{s} = \frac{s_e + s}{s_e} \tag{3}$$

$$\tilde{t} = \frac{t_e + t}{t_e} \tag{4}$$

Bourouiba et al.[37] defined the virtual origin, as described by equations (5) and (6)

$$s_e = \left(\frac{Q_p}{\eta}\right)^{\frac{1}{3}} \cdot \frac{1}{\alpha} \tag{5}$$

$$t_e = \frac{\rho_p Q_p^{\frac{4}{3}}}{(4+C)\alpha M_p \eta^{\frac{1}{3}}} \tag{6}$$

The main puff quantities are the puff volume Q_p and the puff momentum M_p as reported in equations (7) and (8)

$$Q_p = \Omega_p v_p t_{inj} \tag{7}$$

$$M_p = \rho_p Q_p v_p \tag{8}$$

where t_{inj} is the puff injection time at the uniform velocity v_p and ρ_p is its density. Moreover, in the puff model, the drag effect is also considered through the term C, defined as in equation (9)

$$C = \frac{C_D \beta}{2\eta\alpha} \tag{9}$$

where the drag coefficient can be calculated according the Schiller-Naumann model,[38] as described by equation (10)

$$C_D = \frac{24}{\mathrm{Re}}(1 + 0.15\mathrm{Re}^{0.687}) \tag{10}$$

where the Reynolds number is defined as in equation (11)

$$\mathrm{Re} = \frac{\rho_p v_p D}{\mu_p} \tag{11}$$

with D the injection diameter of the source, while the main model constants are $\alpha = 0.1$, $\beta = \pi$ and $\eta = 4/3\pi$. The exact solution of the governing equations (1) and (2) is reported in equation (12)

$$\tilde{s}(\tilde{t}) = \tilde{t}^{\frac{1}{(4+C)}} \tag{12}$$

This solution is valid for $r_m = 0$ (by neglecting the decreasing mass of the ejected droplets due to the evaporation), for $A \ll 0.01$ (i.e. for a density difference negligible between air and puff, due to their temperature difference of 10°C). Then, this solution has a good accuracy for $0.39 < s_e < 1$ and $0.01 < t_e < 0.21$; out of this range, the model is not recommended.

To have a more complete comparison and validation, the CFD model has been also referred to the experimental work.[36] A cough box, with a circular opening to simulate a human mouth, was pressurized to have a controlled cough jet at a discharge velocity of 6 m/s; the duration of the cough jet was 1 s. Small water particles of O (1 μm) were sprayed by a Collison nebulizer. These flow characteristics were shown to be perfectly coherent with the limits of the previous puff theory. The experimental axial distance from the puff tip to the particle injection mouth was measured through one-dimensional hot wire anemometer at the centre section plane (76 position) downstream the cough jet and a hot-sphere anemometer.

Lagrangian CFD particle transport phase

In the CFD approach, the water droplets are treated as a discrete particle. The force acting on each particle is the sum of the drag force and buoyancy force due to gravity on the particle. The particle motion can be described by equation (13)

$$m_P \frac{dv_P}{dt} = F_D + F_B \tag{13}$$

where the forces components are reported in equations (14) and (15)

$$F_D = \frac{1}{2} C_D \rho_F A_F |v_F - v_P|(v_F - v_P) \tag{14}$$

$$F_B = (m_P - m_F)g = m_P\left(1 - \frac{\rho_F}{\rho_P}\right)g = \frac{\pi}{6} D_P^3 (\rho_P - \rho_F)g \tag{15}$$

Eulerian CFD: Inhomogeneous multiphase VOF

The water dispersed fluid evolution in the continuous air was simulated using the volume fraction model (VOF) in an Eulerian approach. The inhomogeneous momentum conservation, by neglecting the interphase mass transfer, is described by equation (16)

$$\frac{\partial}{\partial t}(r_\alpha \rho_\alpha v_\alpha) + \nabla \cdot [r_\alpha(\rho v_\alpha \otimes v_\alpha)] = -r_\alpha \nabla p_\alpha + \nabla \cdot \left\{ r_\alpha \mu_\alpha \left[\nabla v_\alpha + (\nabla v_\alpha)^T \right] \right\} + M_\alpha \quad (16)$$

where M_α describes the interfacial forces acting on phase α due to the presence of other phases. Then the continuity is governed by equation (17)

$$\frac{\partial}{\partial t}(r_\alpha \rho_\alpha) + \nabla \cdot (r_\alpha \rho_\alpha v_\alpha) = 0 \quad (17)$$

and finally, the volume fractions sum is constrained to unity, as in equation (18)

$$\sum_\alpha r_\alpha = 1 \quad (18)$$

It can be combined with the phasic continuity relationship to obtain the transported volume conservation, as in equation (19)

$$\sum_\alpha \frac{1}{\rho_\alpha} \left[\frac{\partial}{\partial t}(r_\alpha \rho_\alpha) + \nabla \cdot (r_\alpha \rho_\alpha v_\alpha) \right] = 0 \quad (19)$$

CFD models

A confined room with an air conditioning system, that includes an inlet grille and an exhaust grille to change air, was modelled. Figure 1 shows the layout of the room having dimensions 5×3 m and a height 3 m. The two grilles have a rectangular form of 0.125×0.5 m. They are placed at the centre line, respectively, near the ceiling (inlet grille) and near the floor the other. The mouth was modelled according to the experimental work of Liu and Novoselac,[36] with a diameter of 0.024 m and located at 1.6 m height from the floor, on the opposite wall from the air conditioning vents. This mouth expelled with a prescribed velocity, water droplets dispersion from the coughing or breathing.

The geometry was discretized using ANSYS ICEM CFD software with a structured multi-block grid, with an O-grid block around the mouth. Figure 2 shows the mesh made with the details of the mouth.

The global mesh dimension, after a grid sensitivity analysis, is about 2 millions of cells (the cells size varies from a minimum of 1.5 mm near the mouth and the walls to a maximum of 50 mm). A value of y+ around 30 is guaranteed at the wall for the safe use of the wall functions in the RNG k-ε turbulence closure. The wall treatment with this turbulence model was chosen based on authors' experience,[32–34] in order to save computational resources and for its stronger numerical stability. This turbulence model is widely used to simulate flows of engineering interest, and it is therefore one of the best validated models available. It provides accurate results in situations with modest boundary layer separations without rotating domains like those considered in the present study. The use of validated wall functions allows the generation of a coarser mesh with respect to the low Reynolds approach for wall turbulence modelling, that is needed for other application fields, like aeronautics or turbomachinery. Attention was focused

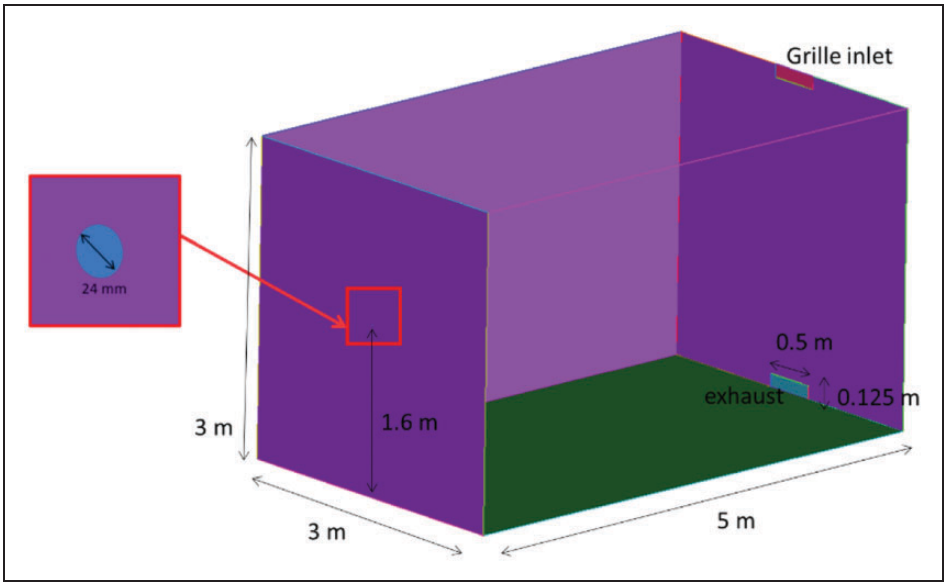

Figure 1. Geometric scheme of the confined room.

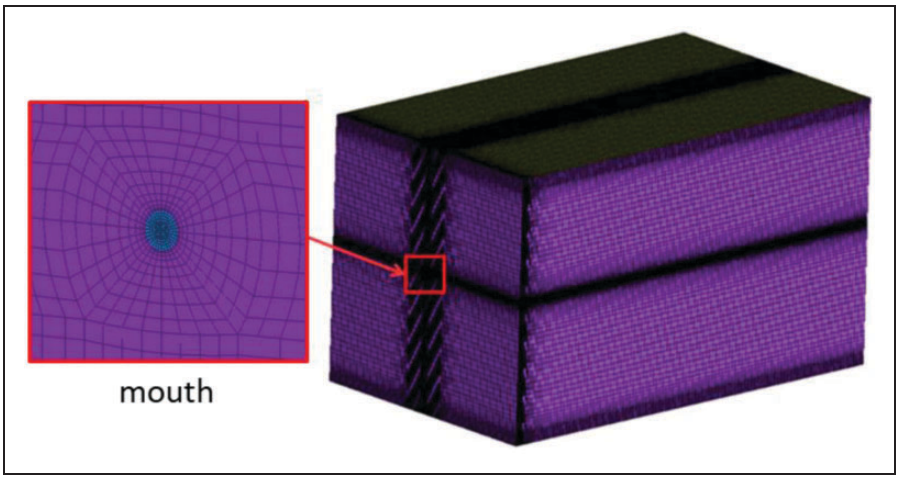

Figure 2. Mesh of the confined room with details grid of the mouth.

on the first mesh cell centre to be in the log-law region.[39]

The numerical model has been set in the ANSYS CFX software. A multiphase model was used to simulate the water particles released from the mouth into the room with ambient air. In this first case, a Lagrangian approach was chosen with a particle tracking model: an ambient air ideal gas (assumed as a continuous fluid) and water with the 'particle transport fluid' morphology with a specified diameter distribution. As regards, the energy equation, the total energy model was used for the air, while the particle temperature model was adopted for the water. Between the two phases, the buoyancy effects were also considered, using the density difference model and using the density of the primary fluid (air) as a reference. The water particles were fully coupled to the continuous fluid to exchange momentum with the continuous phase, enabling the continuous flow to affect the particles, and the particles to affect the continuous flow. The surface tension between air and water was considered through the coefficient 0.073 N/m. Then, the drag force between the continuous phase and the particle phase was modelled with the Schiller-Naumann model, suitable for simulating sufficiently small fluid particles that may be considered spherical.[38] Finally, the Ranz-Marshall[40] model for the heat exchange between the two phases was used together with the homonymous correlation for the continuous phase and a zero resistance on the particle phase side of the phase interface.

Unsteady simulations were performed with a total time of 4 s, and they were initialized in a quiet ambient room at $T = 25°C$. The boundary conditions, reported in Figure 3, consist of an inlet condition where it is fixed: an uniform velocity for 1.0 s, an average turbulent intensity $I = 5\%$ and a water particle population with a normal distribution having an average particle diameter of 5 μm and a standard deviation of 2 μm, at $T = 35°C$. The normal distribution reported to the right in Figure 3, is similar to others from literature.[12] It is representative to simulate the smaller water particles released during a respiratory event that can stay in the ambient air and travel to longer distances than larger particles whose ballistic trajectory is dominated by the gravity making them to fall in a short space. In the inlet grille, a zero velocity condition (no air conditioning in reference case) and an ambient pressure outlet condition were set for the exit section. All the walls were set with adiabatic no-slip condition. Finally, all the equations were solved with the second order numerical scheme. In Table 1, the initial and boundary conditions are summarized.

A grid dependency analysis using three different mesh sizes was performed. In Figure 4, the axial temporal evolutions of the water particles emitted during the same cough event have been reported for the three configurations. In Table 2, the global mesh size of the three meshes are reported, with their maximum axial penetrations of particles after 4 s and the percentage deviations from the case with the mesh immediately before with a coarser grid. The axial penetration of the particles was obtained from the iso-clip, at the mid-plane, where the water particle concentration, defined in the following, is greater than 1%; then, the maximum horizontal coordinate in the above iso-clip was used for the analysis at each time interval.

From the grid dependency analysis, the configuration M2 with 2 million of cells is the most adequate to be used as reference.

Cough event validation

A first simulation set with different cough velocities was carried out, in order to compare the CFD model with the puff theory and with the experimental values.

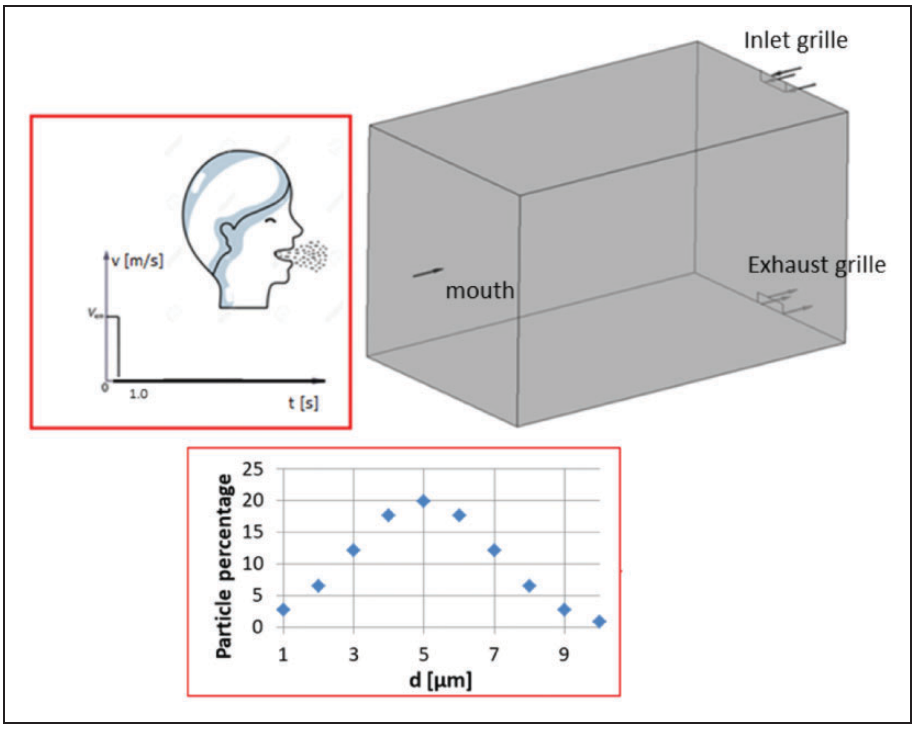

Figure 3. CFD domain with boundary conditions and diameter distribution of the water particle emitted.

Table 1. Initial and boundary conditions imposed for the cough event validation.

Patch	Conditions
Initial cond.	Quiet ambient at T = 25°C
Mouth	Uniform velocity for t = 1 s; I = 5%; water particle diameter normal distributions; T = 35°C
Inlet grille	Zero velocity
Exhaust grille	Outlet ambient pressure
Walls	Adiabatic no-slip

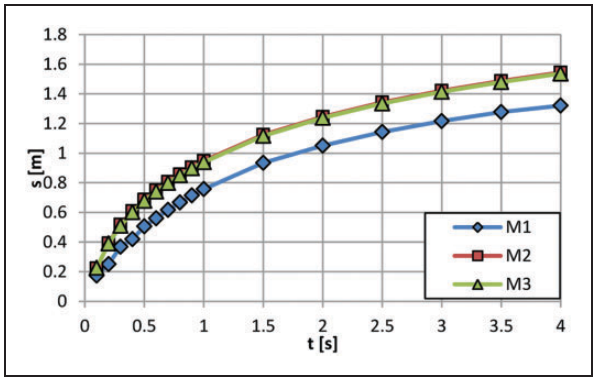

Figure 4. Water particle axial penetration with time – grid dependency.

Table 3 summarizes the cases with the cough velocities considered.

In Figure 5, the temporal axial penetration of the puff tip from the injection particle mouth is shown at the different cough velocities, for the different approaches. The axial penetration from the puff theory was calculated through equation (12).

In Table 4, the maximum puff axial penetration at 4 s for different cases with the percentage errors with respect the puff theory are reported.

The CFD model is perfectly able to identify the water particles path, by predicting their final position with a good accuracy. Low errors were encountered in comparison with the puff theory, and a faithful trend over time was detected. For Case 2, a comparison with the experimental trend was also possible. If the theoretical model and the CFD model have negligible error, the experimentation overestimates the axial distance by 20%. However, the trend in the considered period is completely comparable with the two numerical models. In particular, the axial distance follows in all cases a power function, with an exponent slightly higher (equal to 0.5) in the experimental case. Finally, Figure 6 shows the distributions and the particles path (in grey) after

Table 2. Mesh configurations used for the mesh sensitivity with their axial penetration of the water particles after 4 s and the percentage deviations from the previous case with a coarser grid.

Mesh	Cell number M cells	Axial penetration after 4 s in (m)	Percentage deviation from the case with a coarser grid
M1	1.2	1.320	–
M2	2.0	1.544	+14.50
M3	2.9	1.536	–0.51

Table 3. Simulation set of coughing.

Case #	Particle injection velocity (m/s)
1	3
2	6
3	12

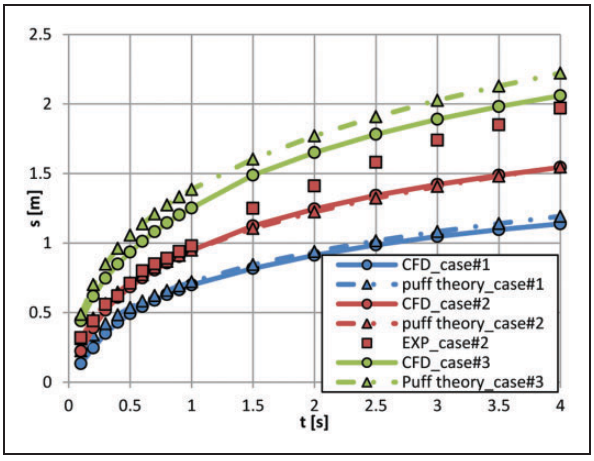

Figure 5. Comparison of the CFD model with respect the reference works of the water particle axial penetration along the time, at different cough velocities.

4 s, superimposed on the velocity contour at the room mid plane, for the three simulated cases.

Without air conditioning, the water particles emitted by a cough have an almost horizontal trend, showing how the different simulated cough velocities are similar to the puff theory within its validity limits. In the experimental case, the axial distance overestimation can be due to the difficulties in measuring the puff boundaries and the axial distance using anemometers.

Breathing event validation

The previous CFD model with the same equations for the cough event was applied to the simulation of normal breathing, with the only difference of the mouth dimension and the boundary conditions described below. A room with the same geometrical dimensions was used, with a mouth area of 41.7 mm^2, in order to compare the numerical results to the Zhao et al.'s work.[41] Moreover, in this case, an unsteady inlet condition was set at the mouth to simulate the cyclical exhalation and inhalation phases with a triangular wave trend as in the Zhao et al.[41]

Figure 7 shows the trend of the two simulated breathing cycles (8 s) having peaks of emitted velocity of 6 m/s and a period of a breathing cycle of 4 s. The particles are emitted from the mouth with an inclination of 30° with respect to the vertical face wall (in order to simulate breathing from the nostrils). The same turbulence intensity (I = 5%) from the mouth has been retained as for the cough event; both respiratory events are in the range Re = 5000–17,000 for which the empirical correlation of the pipe flows predicts a medium turbulence intensity.[42]

The average particles diameter was fixed again equal to 5 μm. In this case from the inlet grille, a uniform velocity condition with turbulence intensity of 10% was also set to simulate the ventilation system of the room and an output mass flow rate was imposed at the exhaust grille to guarantee the correct ACH (air change per hour). In Table 5, the boundary and initial conditions imposed for the breathing event validation are summarized.

The unsteady simulations have been initialized with a steady run with air conditioning and no breathing. The water particle evolutions in the room mid-plane (at different instants) obtained by the CFD simulations, were compared with those available in publication.[41] The comparison results are shown in Figure 8.

Also, in this case, the CFD model has obtained a distribution of the emitted particles almost similar to the concentration distribution obtained in the literature case. From left to right, the particles during the exhalation phase (after 0.5 and 1 s) are initially placed near the emitting mouth and then spread, but still in a very restricted region placed at a maximum distance of 0.5 m from the mouth. In the figure on the far right, at the instant 2.5 s relative to the inspiration peak, the previous emitted particles have largely already fallen to the floor within a maximum distance of 1 m from the mouth; only a minimal part of the water particles is reabsorbed from the mouth. Therefore, in comparison to the coughing cases, the interpersonal distance of 1 m

Table 4. Comparison of the axial penetration of the water particles after 4 s.

Case	Approach	Axial penetration after 4 s in (m)	Error, %
Case#1 (3 m/s)	CFD	1.14	4.2
	Puff theory	1.19	–
Case#2 (6 m/s)	CFD	1.54	0.64
	Puff theory	1.55	–
	Experimental	1.97	21.3
Case#3 (12 m/s)	CFD	2.06	7.2
	Puff theory	2.22	–

CFD: computational fluid dynamics.

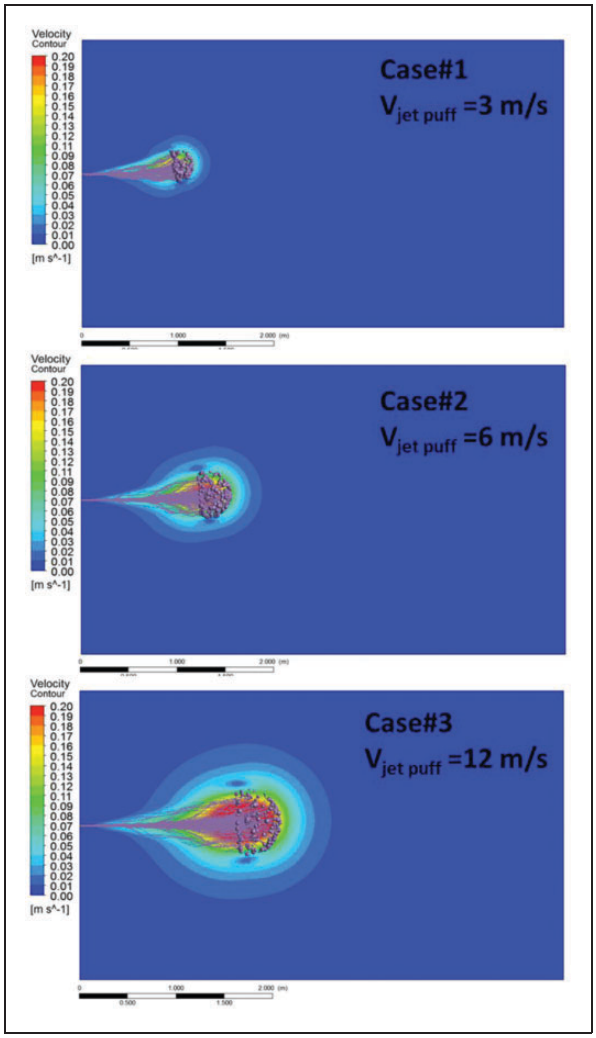

Figure 6. Velocity contours and water particle distribution at room mid plane for the three cases after 4.0 s.

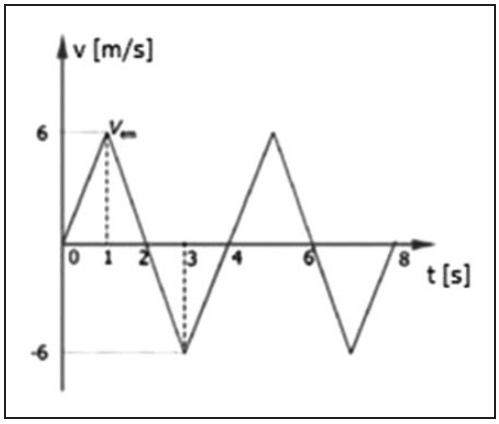

Figure 7. Two breathing cycle, according Zhao et al.[41]

in this case can be better assumed as the more adequate. In fact, in this case, the flow structure of the room is also affected by the ventilation and the water particles emitted with a certain inclination are stretched to the floor before of 1 m axial distance from the mouth. However, some differences are detected between the CFD model and the reference contours; after 2.5 s, some water particles fall to the floor, while in the reference case, they reach only the height of 0.5 m from the ground. This mismatch can be due to the more severe limitations of the numerical model used in the reference with respect the CFD model adopted in this paper. In the reference, a simple N-point air supply opening model with a zero equation turbulence model was adopted.[41] Moreover, in the present paper, a particle diameter distribution (Figure 3) was considered with respect to the uniform diameter distribution (with a lower value) used in the reference. Despite these differences in the numerical models, a good overall match was observed, and the present CFD approach can be considered acceptable for the breathing event also. The velocity contours show that the red velocity area is located at a height above 0.5 m and confirmed that the same area influenced by the cough or breathing from the mouth was obtained with the two approaches.

Analysis of the air conditioning – Breathing

The influence of the air conditioning system in the room on the water particles diffusion was analysed

Table 5. Boundary and initial conditions imposed for the breathing event validation.

Patch	Conditions
Mouth	Unsteady velocity; flow inclined of 30°; I = 5%; water particle diameter normal distributions; T = 35°C
Inlet grille	Inlet uniform velocity; I = 10%; T = 25°C
Exhaust grille	Outlet mass flow rate
Walls	Adiabatic no-slip
Initial cond.	Flow structure of the ventilation with the appropriate ACH without the breathing from the mouth

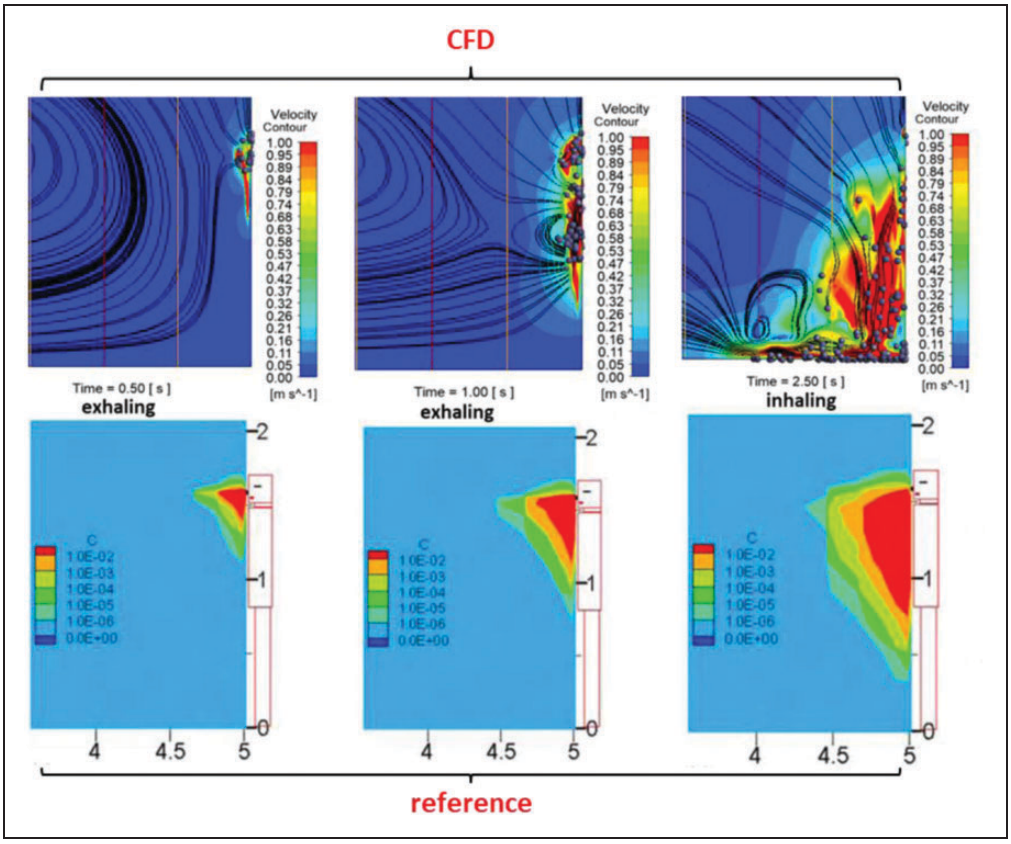

Figure 8. Comparison of the CFD model (upper) with respect to Zhao et al.[41] (lower) of the water particle diffusion in the room mid-plane at different instants – breathing.

Table 6. Simulation set of breathing – main parameters.

Case #	Velocity inlet @Inlet grille (m/s)	Outlet mass flow rate @exhaust grille (kg/s)	ACH
1	0.1	0.007	0.5
2	1.0	0.074	5
3	2.0	0.148	10

ACH: air change per hour.

for the breathing case. In Table 6, the simulation dataset with the inlet velocity at the inlet grille, the mass flow rate imposed at the exhaust grille and the corresponding ACH are reported.

In order to visualize the main effects of the conditioning system on the release of water particles from the mouth during the normal breathing, the water particle diffusion at the room mid plane of the three cases after 8 s, was considered and are shown in Figure 9.

After two cycles of normal breathing (8 s), the saliva particles emitted are located at a height below 1 m in all cases. In fact, the macro flow recirculation in the room and the low momentum of the particles tend to fall back quickly towards the floor. However, from left to right, by increasing the ventilation (from a simple air exchange to a more marked forced ventilation), the velocity contours show that the air jet released by the inlet grille is reflected on the opposite wall to fall backwards to the floor with an increasing force. The water particles are dragged for a longer distance as the ACH increases. This application confirms that the normal

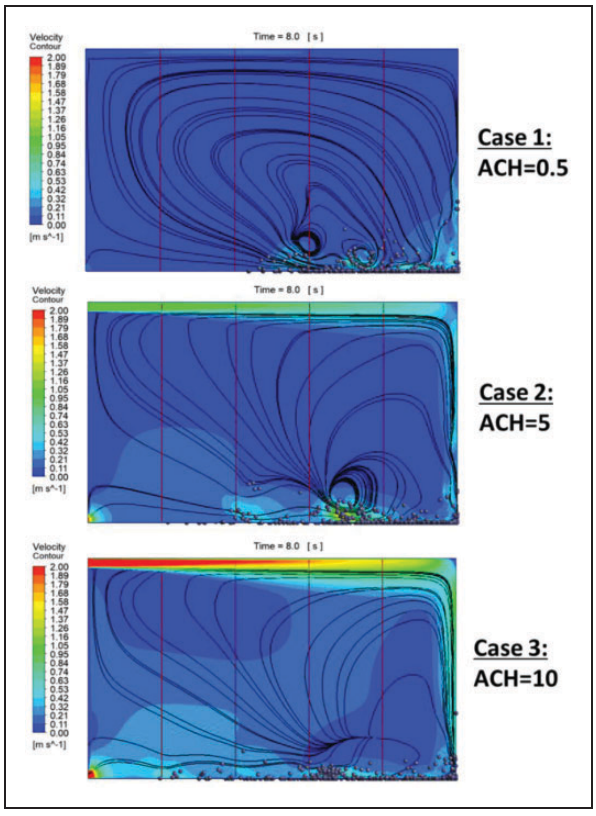

Figure 9. Water particle diffusion at room mid-plane after 8 s at different ACH – breathing.

breathing covers shorter distances than coughing despite a stronger ambient ventilation. To have a more detailed view of the evolution and concentration of the water particles, in Figure 10, the concentration trends are reported at different distances from the mouth over time.

This concentration was measured using the following C parameter through the particle number rate, as described in equation (20)

$$C = \frac{\dot{N}}{\int \dot{N}_{mouth} \cdot dt} \times 1000 \qquad (20)$$

In Case 1, most of the particles after just 4 s have passed the control plane placed at one metre from the mouth, and after 6 s, they flow through the plane at 2 m. In the meantime, the delayed particles are still crossing the first plane. With stronger ventilation (Case 2) after about 4.5 s, the particles have already reached the plane at 2 m in a similar percentage to those placed on the first plane. Finally, at 3 m, a small variation on the concentration line can be noted. For Case 3 (ACH = 10), the peaks of the planes at 1 and 2 m have lower values, because, as reported also in the Figure 9, the stronger ventilation effect drags the water particles and stretches them to the ground without droplets accumulation. Therefore, the particles reach the first and the second control plans in a shorter time. Moreover, the percentage of water particles that reaches, at the same instant, the plane located at 3 m from the mouth, is double with respect to Case 2 (ACH = 5).

Two persons in a meeting room

Following the previous basic use of the Lagrangian numerical model for the simulation of the water particle diffusion emitted during the breathing and coughing, a more applicative case has been developed. In a meeting room with an air conditioning system, there are two persons sitting in front of a table. The emanations from their noses were set with a prescribed velocity and water droplets distribution. Figure 11 shows the geometrical scheme of the case with the main dimensions. The upper part of the model body is reported in detail with the patches of the nose and mouth.

The room has a size of 3×3.5 m and a height of 2.5 m. Two persons were seated at a table, placed at the centre of the room, facing each other. Their mouths were placed 1.2 m from the floor. The grilles (inlet and exhaust) for ventilation are both located near the ceiling, one above the other and directed towards the long side of the room, modelling an ordinary wall-mounted air-conditioner (splitter type).[7] The size of each grille is 0.7×0.05 m. Finally, the nose and the mouth of each body have a circular area of 330 and 350 mm^2 respectively, according the mannequins characteristics used by Zhu et al.[7] Figure 12 shows the mesh created for the case described above with some details.

An unstructured mesh of about 2.6 millions of cells with a minimum size of 2 mm (located on the body) and a maximum of 100 mm was used for the modelling. The prism layer was created on all the surfaces (including the two persons) in order to obtain a value of y+ around 30. This application was calculated with two different approaches to simulate the breathing phases: (1) Lagrangian for the evolution of a water particle population and (2) Eulerian, for the formation and evolution of water aerosols from the breathing phases.

Lagrangian approach

The Lagrangian CFD model is similar to the one described above for the basic case with small differences. It consists of a multiphase model with particle tracking having air as a continuous fluid and water, as a particle transport fluid. The k-ε turbulence model is confirmed. The temperature variations were also considered, and the energy equation was solved for

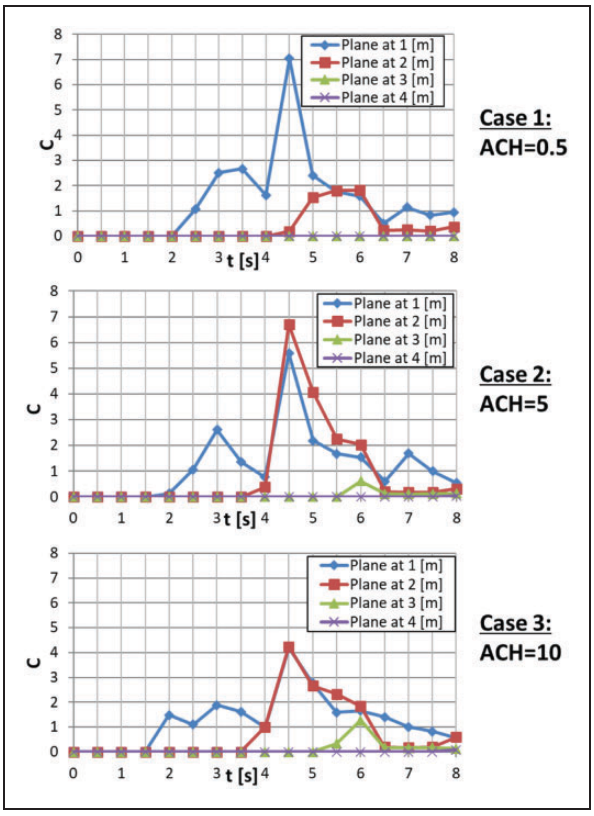

Figure 10. Water particle concentration over time at several control plans for different ACH – breathing.

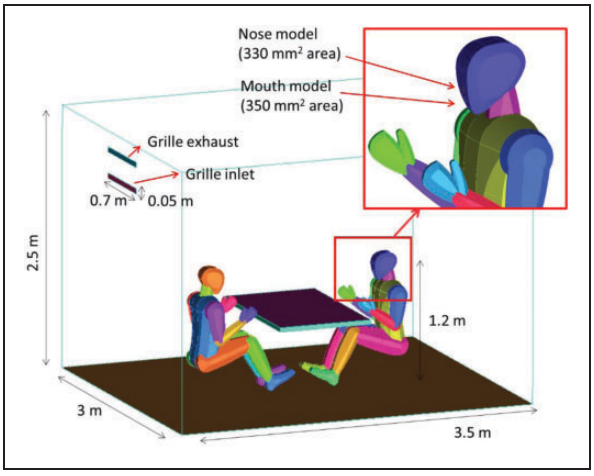

Figure 11. Geometrical scheme of the conference room with two persons and detail on the model body.

the air and the water particles. The Ranz Marshall model for the heat exchange between the two phases was used together with the homonymous correlation for the continuous phase and a zero resistance on the particle phase side of the phase interface. The density difference model was activated for the buoyancy effect

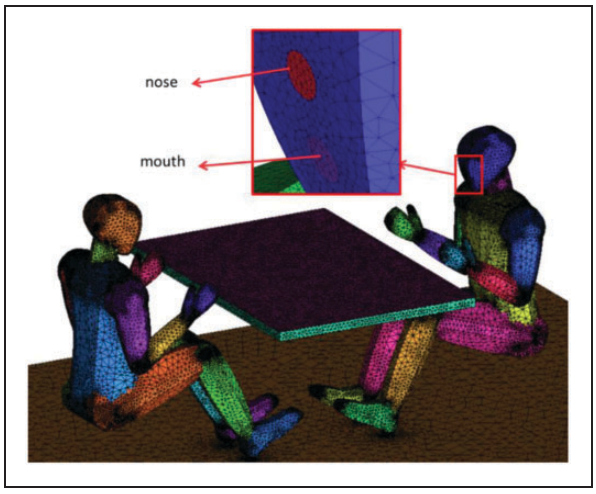

Figure 12. Mesh of the meeting room – two persons with face details.

between the two phases and the Schiller Naumann model for inter-phase drag.

The simulations were carried out to simulate two breathing cycles for each person (8 s) out of phase by half a period (2 s) with corresponding velocity profile of Figure 7. The diameter of the particles was considered uniform equal to 5 μm at a temperature of 32°C. A uniform diameter distribution with the order O (1 μm) was adopted taking into account the data from the Yang distribution.[12]

With the above diameter, the particles are dragged by the main flow field resulting in a stronger effect of particle motion and in the ambient. The motion of larger particles is dominated by gravity and the effect of the indoor flow distribution on their path is negligible. To evaluate the gravity role on the particles trajectory, the Stokes number $St = \tau_P/\tau_F$ can be used, where the kinematic time scale of the droplets is $\tau_P = \rho_P D_P{}^2/(18\nu_F\rho_F)$. For a magnitude order O (1 μm), the result is $\tau_P < 1$ μs, while the fluid dynamic time scale is $\tau_F > 1$ s. It follows that these particles are dominated by transport phenomena rather than by gravity. For the above reasons, the use of a uniform diameter can be justified. All the walls were set as adiabatic no-slip, while a heat flux of 23 W/m^2 was imposed at the body surfaces to simulate the heat released by an adult man at rest.[7] Uniform velocity was set at the inlet grille for the ventilation, with a temperature of 26°C and a turbulence intensity of 10%. At the exhaust grille, a mass flow rate condition was set to guarantee the correct ACH. In Table 7, the initial and boundary conditions imposed for the meeting room application are summarized.

Table 8 shows the main parameters of the ventilation system of the two cases. In Case 1, the ventilation was set to ensure a normal air exchange, while in Case

Table 7. Initial and boundary conditions imposed for the meeting room application.

Patch	Conditions
Noses	Unsteady velocity; I = 5%; uniform water particle diameter distributions; T = 32°C
Inlet grille	Inlet uniform velocity; I = 10%; T = 26°C
Exhaust grille	Outlet mass flow rate
Men	Uniform heat flux of 23 W/m^2K
Walls	Adiabatic no-slip
Initial cond.	Flow structure of the ventilation with the appropriate ACH without the emission from the noses

ACH: air change per hour.

Table 8. Simulation set of breathing in conference room at different ACH – main parameters.

Case #	Velocity inlet @Inlet grille (m/s)	Outlet mass flow rate @exhaust grille (kg/s)	ACH
1	0.4 (normal to boundary)	0.0166	2
2	2.07 (inclined of 60°)	0.0854	10

ACH: air change per hour.

2, the air flow was modified and inclined by 60° with respect to the vertical wall, in order to impact the centre of the table with a higher velocity.

Figure 13 shows the water particle diffusion at room mid plane at different instants (2–3–4 s) for the two cases considered.

In the three figures on the left (ACH = 2), the alternate breathing cycles of the occupants along time are clearly represented. The convective flow field generated by the heat released by each person is evident from the above contours; it can partially influence the trajectory of the emitted particles. The particles tend to accumulate above the table and between the two persons. The air conditioning system of Case 1 has a reduced influence on their motion. An air stagnation region is created between the occupants due to their physical obstruction to the flow from the ventilation system and to the upward convective motion due to body heat release. An increased and properly oriented air ventilation is capable to influence the water particles trajectory to avoid stagnation and recirculation effects.

The room ventilation system can therefore create a barrier for the evolution of the exhaled particles into the ambient and to the other occupant. In this case, the water particles are dragged towards the table and do not hit the face of the opposite seated person being therefore not inhaled. The positioning of the ventilation system and the set up can be rather fundamental to control the diffusion of particles exhaled during a normal breathing to minimize or avoid the risk of contagious infection between occupants.

Eulerian approach

A second approach was developed for the same application. The Eulerian model can be equally representative for the human aerosol emission and transport. Water vapour formed by very fine droplets of O (1 μm) is exhaled from the mouth and its behaviour is dominated by transport phenomena rather than by gravity; it can be transported into the 3 D flow structure with high resident times giving a high contagion risk.[43] Some reference works use this numerical approach to represent the scenarios of the distributions of coughed droplets in indoor environments,[44] such as in a classroom with a ventilation system.[45,46] This approach has been also used recently to investigate the effects of cough intensity and initial mucus thickness on the mucus transport and clearance in a mouth-to-trachea airway geometry.[47] An inhomogeneous multiphase volume of fraction (VOF) model was set between the air (ideal gas) and water, considered as a dispersed fluid having an average particle diameter of 5 μm. The combination of the SST turbulence closure for the primary fluid with the zero equation algebraic turbulence model for the water dispersed phase was used for its higher numerical stability with respect to the k-ε closure. The total energy equation model was adopted for both phases. The additional setting between the two phases for drag, heat exchange and buoyancy effects, was set in a similar way to those in the Lagrangian approach. Same set of boundary conditions was used with the only difference of uniform VOF value at the mouth and nose sections. Figures 14 and 15 compare the results from the two approaches, respectively, for Case 1 and Case 2 (Table 8), showing the water particle diffusion at the room mid-plane.

The left figures for the Lagrangian model show the velocity contours with the water emitted particles in grey, while for the Eulerian model (right pictures), the water concentration is shown through the water VOF contours. Very similar distributions over time were obtained with the two approaches. For Case 1, in both approaches, the emissions (particles or aerosol)

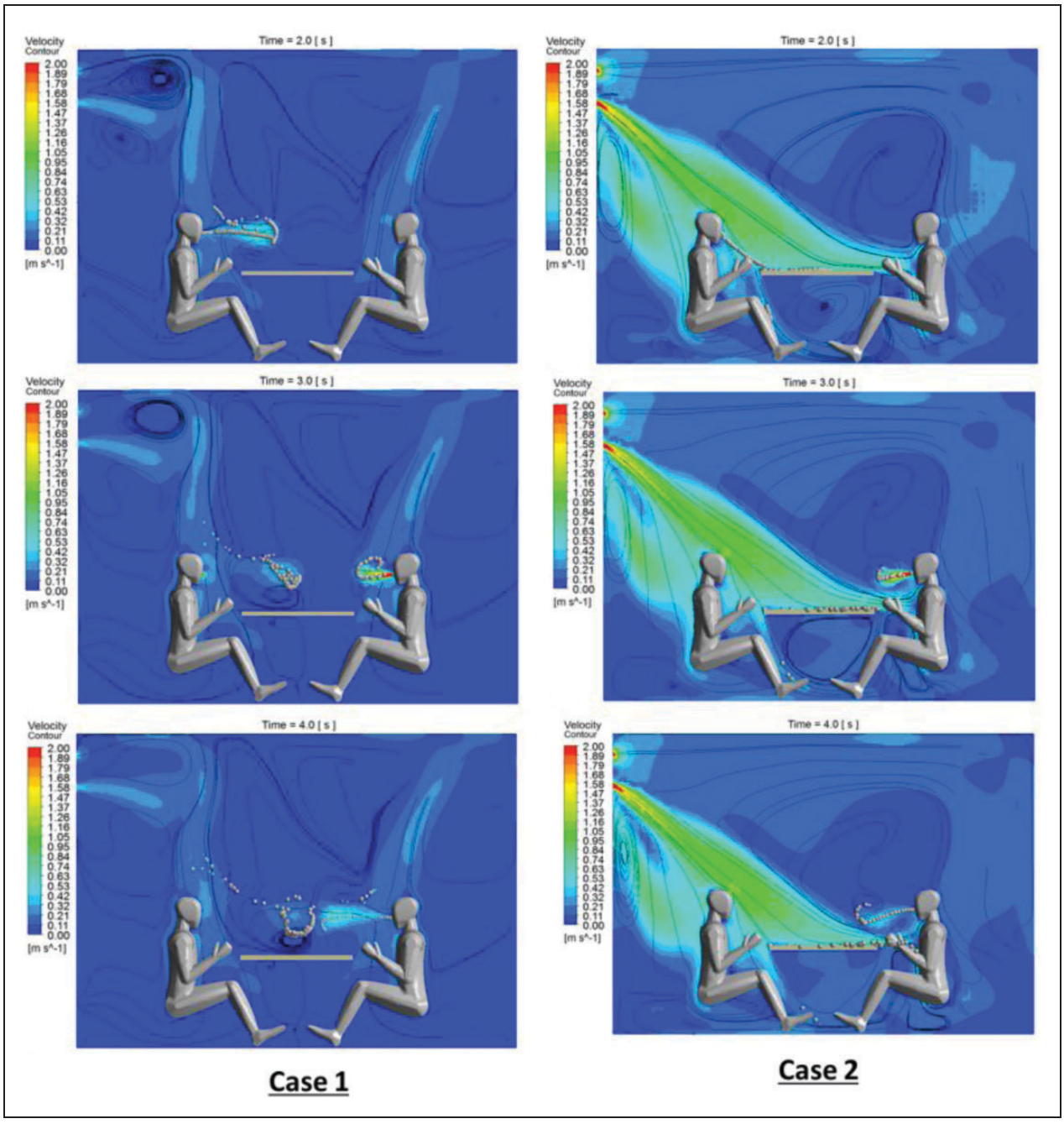

Figure 13. Water particle diffusion at room mid-plane at different time (2–3–4 s). Case 1 (left) and Case 2 (right) – meeting room breathing case with Lagrangian approach.

concentrate above the table and between the two persons, for the mechanisms previously described. For Case 2, in both approaches, it is evident how the exhalation of the first person is dragged by the air ventilation system towards the table and it is diluted, lowering the risk of inhalation by the opposite person. Both models can be effective for the simulation of the exhalation and diffusion of water particles during breathing in a confined room. The Lagrangian approach is more useful to directly detect the trajectory of the particles (which may also have a non-uniform diameter distribution), while the Eulerian approach is effective to predict the aerosols concentration of water vapour from breathing and its evolution from multiple sources and to assess the effect of a protection mask worn by the occupants.

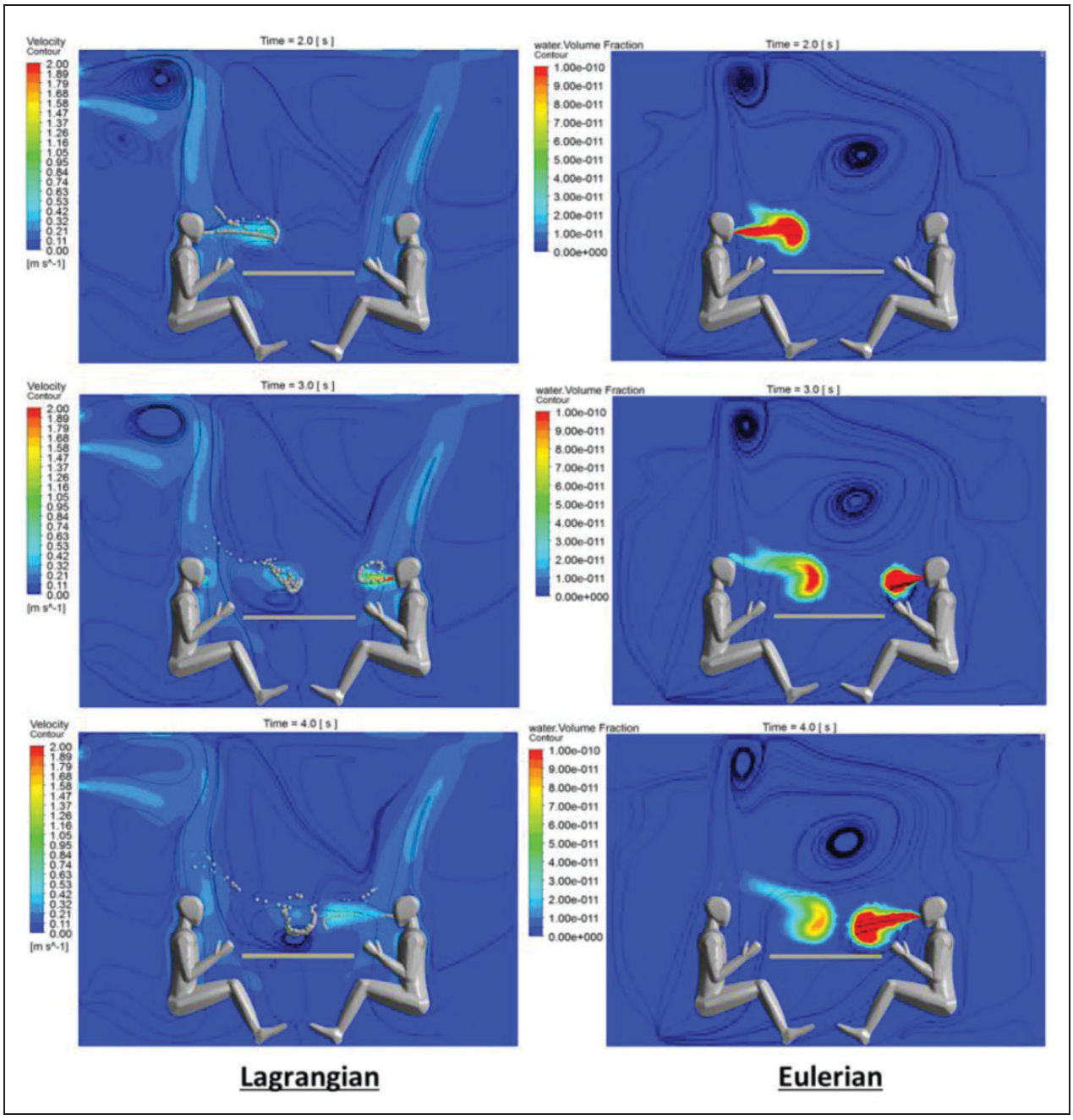

Figure 14. Comparison of water particle diffusion at room mid-plane at different instants. Lagrangian (left) and Eulerian (right) approach – Case 1.

Effect of protection mask

Using the Eulerian approach, a water VOF reduced by 95% was set at the occupant's nose to simulate the use of a common surgical mask (EN 14683 – Type 1).[48–50] In addition, the water vapour flow was inclined of 60° upwards, in order to take into account the deviation that the mask induces to the breathing flow. Figure 16 shows a comparison, relative to Case 1 (Table 8) at the room mid plane, for the water concentration evolution without (left) and with (right) protective mask.

The effect of the protective mask: the water vapour concentration (which remains in the environment) tend to dilute with the air ventilation system until it disappears. In the no-mask case, a water vapour cloud forms between the two persons with dangerous conditions if pathogens are present. With mask protection, the breathing is deflected upwards, interacts with the air

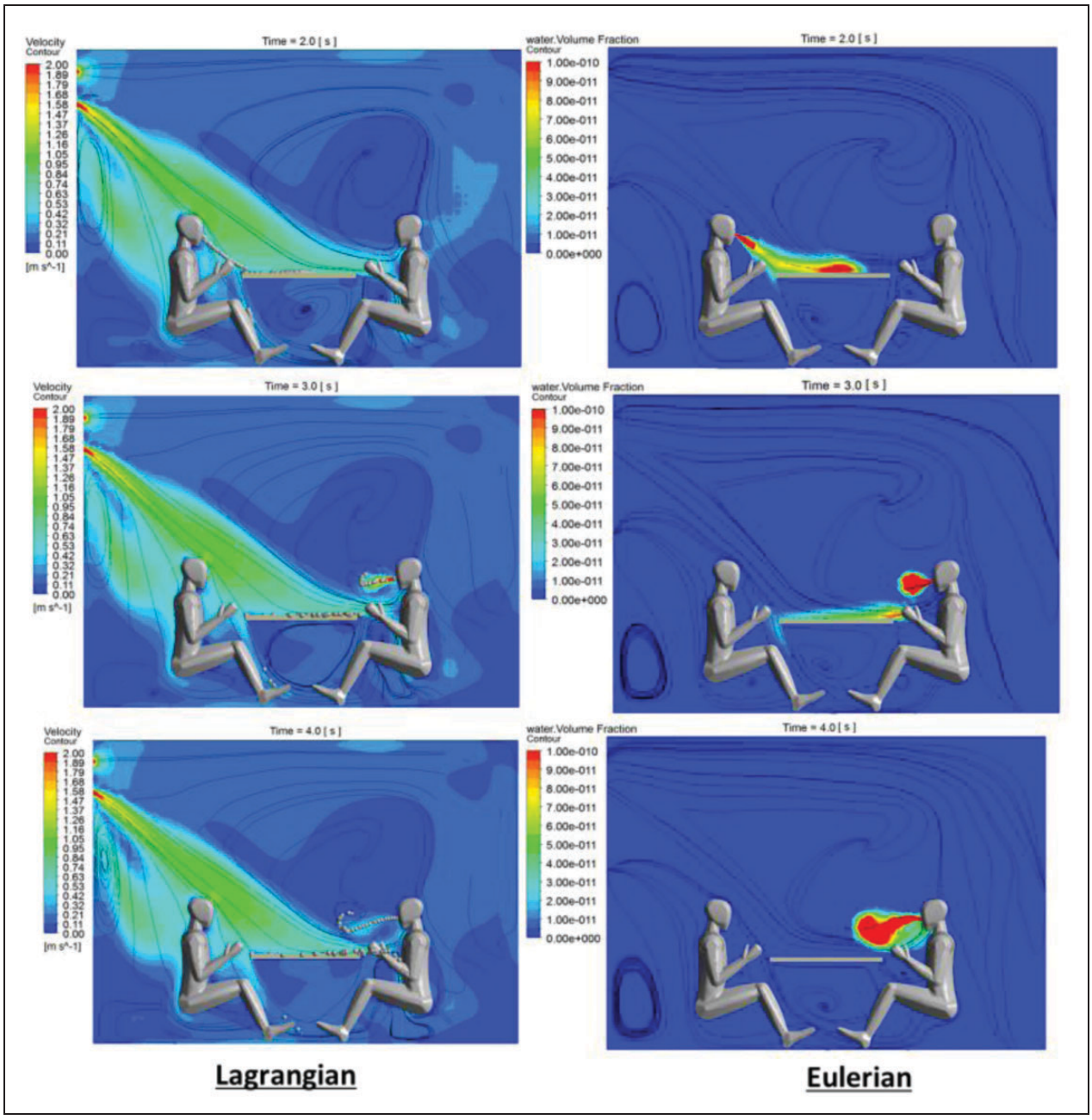

Figure 15. Comparison of water particle diffusion at room mid plane at different instants. Lagrangian (left) and Eulerian (right) approach – Case 2.

conditioning flow toward the ceiling and it is mixed and washed. Similarly, the same comparison is reported in Figure 17 to study the effect of mask protection during coughing.

The cough was set in a similar way to the first paragraph of the validation section, as a water vapour exhalation with a uniform VOF with a velocity of 22 m/s for 0.5 s from the mouth. With a protective mask, the amount of water VOF was reduced by 95% and inclined of 60° upwards.

The importance of using a protection mask is evident also in the case of coughing. The water vapour cloud that would hit the other occupant after 2 s (figure above) with rather high concentrations is diluted and dispersed by the conditioning system with safest conditions for the person in opposite position.

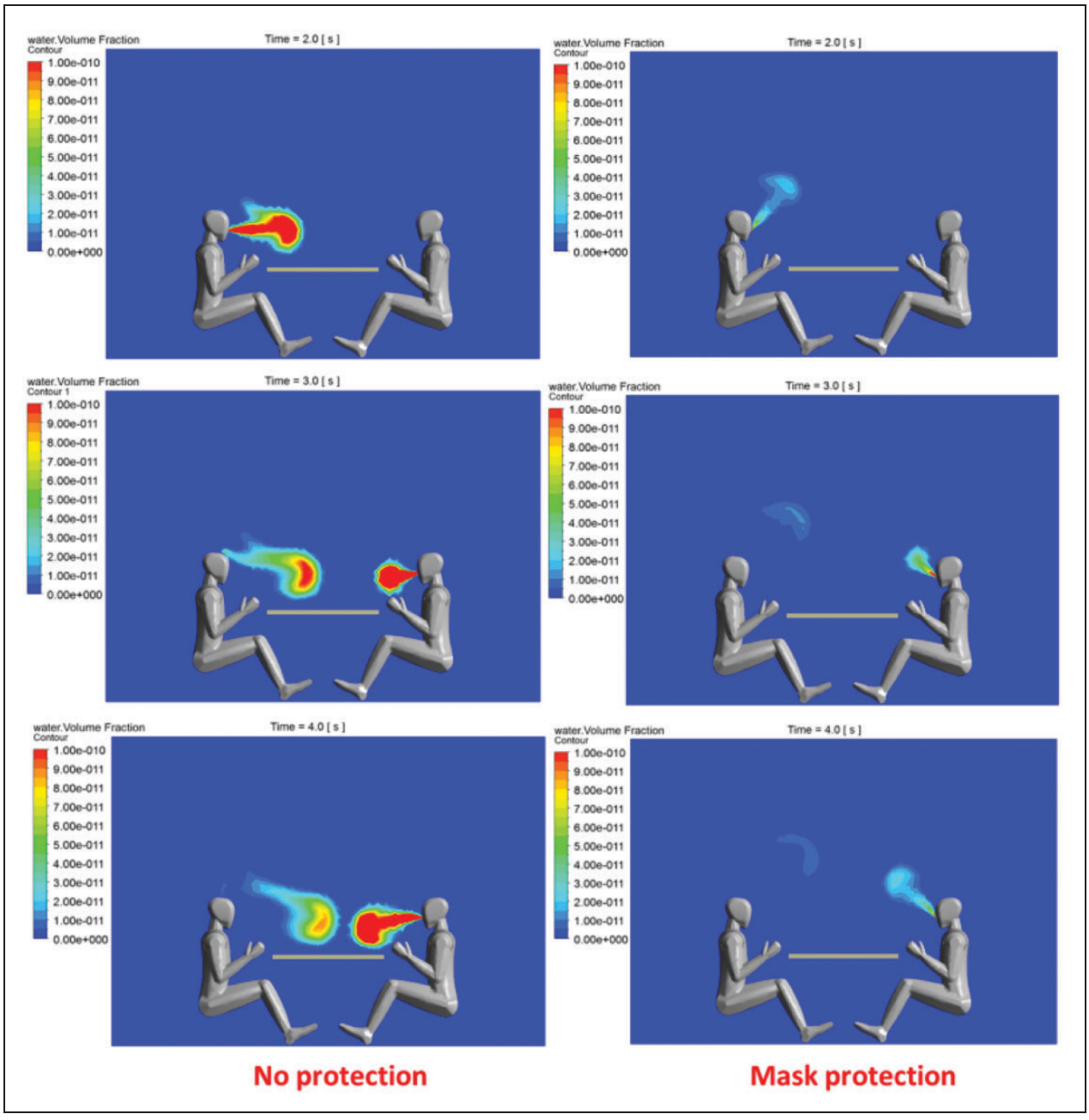

Figure 16. Comparison for no protection and mask protection VOF evolution. Room mid-section – breathing.

Conclusions

The simulation of the saliva particle exhalation during coughing or breathing in an indoor ambient with ventilations system was demonstrated through the use of URANS CFD models. Two different approaches were set up and tested. The Lagrangian is best suited for predicting the trajectory of the emitted particles, while the Eulerian is more effective for simulating the formation of aerosols and for calculating its concentration in the environment. The aim of this paper is to provide an effective tool to study the best use and management of confined spaces with the presence of occupants that can release pathogens through respiratory events. With the simulation approaches, the setup and management strategies of indoor air conditioning and ventilation systems can be supported. In fact, the flow structure generated by a ventilation system can radically change the reference condition of the respiratory puff in the calm ambient air making the

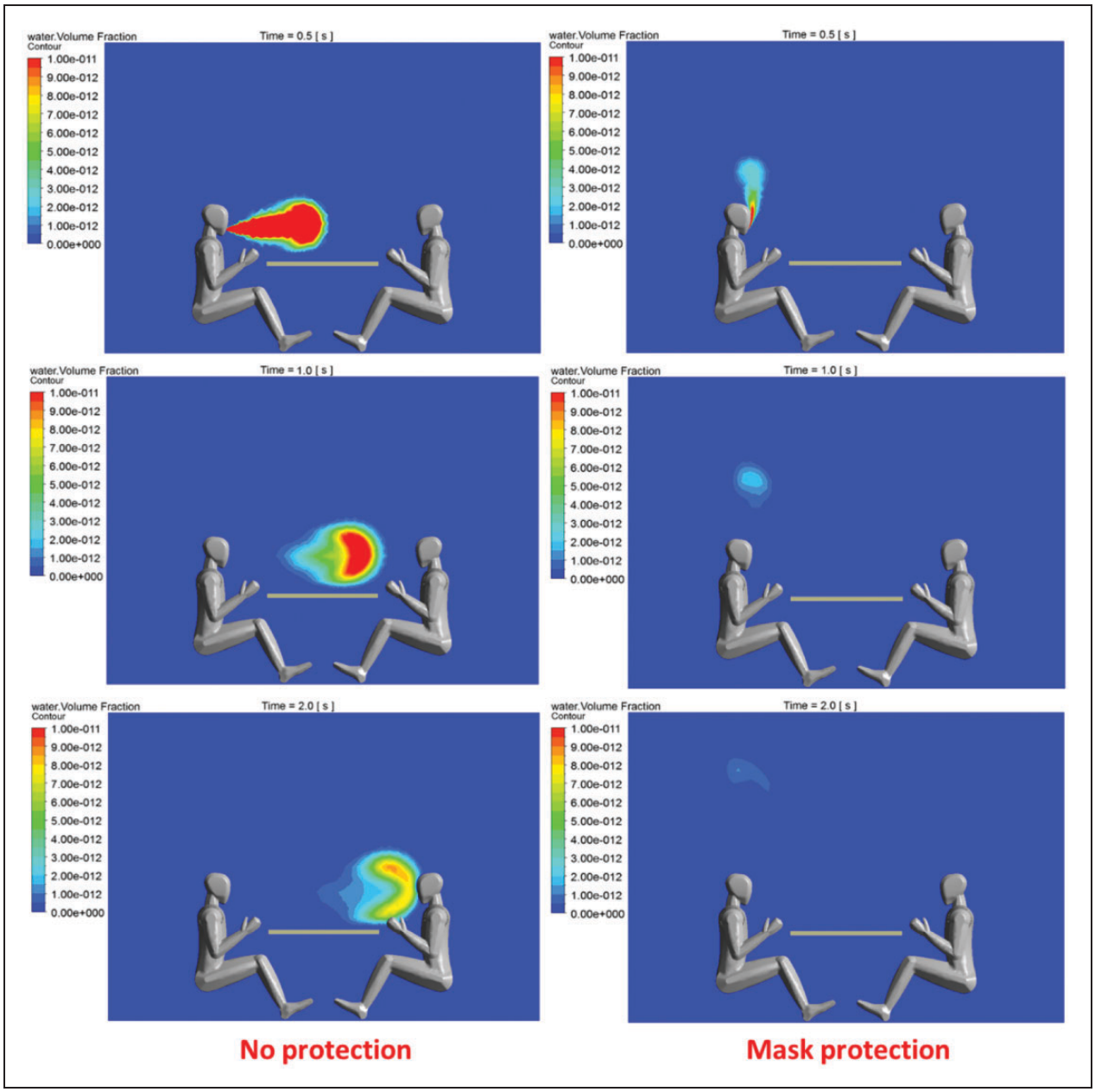

Figure 17. Comparison for no protection and mask protection VOF evolution. Room mid-section – coughing.

analysis of the safety conditions for occupants very much related to the actual indoor air distribution. The interpersonal distance of 1 m can or cannot be enough as a reference rule depending on the local flow structure. The proposed CFD pragmatic approach can be accurate enough for the respiratory puff evolution, with respect to more complicated and computationally heavy approaches,[30] and can be efficiently used to simulate actual conditions of indoors flow structure. It can be considered as an effective tool for the indoor ambient management strategy in safety conditions with respect to the pathogen risks, especially in this COVID-19 pandemic.

The coughing event in an empty room was simulated in order to validate the CFD model by comparing it with the puff theory and experimental data. The same room was used to simulate the breathing event and the results were compared to a reference numerical work. After the model validation in simple reference conditions, a more realistic case of a meeting room with two persons sitting at a table was considered. Different characteristics of the emitted water particles (emission

speed) were considered in coughing to understand their different behaviour and to evaluate its axial penetration. The room ventilation system setup has confirmed its influence on water particles dispersion and diffusion in the room. It is an effective parameter to work with to make an indoor layout safer for the occupants. A useful practical outcome of the simulation approaches is the prediction of the interpersonal distances that can be considered safe in a given situation. A stronger ventilation system can transport to a greater distance the pathogen particles. However, a well-oriented ventilation can even be safer for the occupants. Our results have shown that the use of the Eulerian model can effectively simulate the effect of a protection mask worn by the occupants.

In the YouTube channel of the CFD Group of the University of Genoa,[51] https://www.youtube.com/channel/UCHa_j6PpCPJxBhcVAP1neRw, the videos of the simulations carried out in this paper have also been published, for easier understanding and visualization of the results described above. The models are currently applied to the simulation of public transportation safety and management to minimize COVID-19 infection to the passengers. An application is also showed in the above channel.

Authors' contribution

All authors contributed equally in the preparation of this article.

Acknowledgements

The scientific support and discussions with the colleagues from the University of Genova Prof. Maurizio Ferretti, Dr. Valentina Caratto, Dr. Lorenzo Ball, Prof. Paolo Pelosi and Dr. Stefano Alberti are greatly acknowledged.

Declaration of conflicting interests

The author(s) declared no potential conflicts of interest with respect to the research, authorship, and/or publication of this article.

Funding

The author(s) disclosed receipt of the following financial support for the research, authorship, and/or publication of this article: POLI MD Srl – Italy – funded this research and their financial support is warmly acknowledged.

ORCID iD

Davide Marsano https://orcid.org/0000-0002-6952-174X

References

1. Walls AC, Park YJ, Tortorici MA, Wall A, McGuire AT and Veesler D. Structure, function, and antigenicity of the SARS-CoV-2 spike glycoprotein. *Cell*. 2020; 181: 281–292.
2. World Health Organization. Modes of transmission of virus causing Covid-19: implications for IPC precaution recommendations: scientific brief. *Technical Report*, www.who.int/news-room/commentaries/detail/modes-of-transmission-of-virus-causing-covid-19-implications-for-ipc-precaution-recommendations (accessed 4 August 2021).
3. Cebral JR and Summers RM. Tracheal and central bronchial aerodynamics using virtual bronchoscopy and computational fluid dynamics. *IEEE Trans Med Imaging* 2004; 23: 1021–1033.
4. Zhang Z and Kleinstreuer C. Transient airflow structures and particle transport in a sequentially branching lung airway model. *Phys Fluid* 2002; 14: 862–880.
5. Nithiarasu P, Hassan O, Morgan K, Weatherill NP, Fielder C, Whittet H, Ebden P and Lewis KR. Steady flow through a realistic human upper airway geometry. *Int J Numer Meth Fluids* 2008; 57: 631–651.
6. Chen C, Lin CH, Jiang Z and Chen Q. Simplified models for exhaled airflow from a cough with the mouth covered. *Indoor Air* 2014; 24: 580–591.
7. Zhu S, Kato S and Yang JH. Study on transport characteristics of saliva droplets produced by coughing in a calm indoor environment. *Build Environ* 2006; 41: 1691–1702.
8. Malve M, Perez del Palomar A, Lopez-Villalobos JL, Ginel A and Doblare M. FSI analysis of the coughing mechanism in a human trachea. *Ann Biomed Eng* 2010; 38: 1556–1565.
9. Rahiminejad M, Haghighi A, Dastan A, Abouali O, Farid M and Ahmadi G. Computer simulations of pressure and velocity fields in a human upper airway during sneezing. *Comput Biol Med* 2016; 71: 115–127.
10. Duguid JP. The size and duration of air carriage of respiratory droplets and droplet nuclei. *J Hyg (Lond)* 1946; 44: 471–479.
11. Fairchild CI and Stamper JF. Particle concentration in exhaled breath. *Am Ind Hyg Assoc J* 1987; 48: 948–949.
12. Yang S, Lee GWM, Chen CM, Wu CC and Yu KP. The size and concentration of droplets generated by coughing in human subjects. *J Aerosol Med* 2007; 20: 484–494.
13. Chao CYH, Wan MP, Morawska L, Johnson GR, Ristovski ZD, Hargreaves M, Mengersen K, Corbett S, Li Y, Xie X and Katoshevski D. Characterization of expiration air jets and droplet size distributions immediately at the mouth opening. *J Aerosol Sci* 2009; 40: 122–133.
14. Ai ZT and Melikov AK. Airborne spread of expiratory droplet nuclei between the occupants of indoor environments: a review. *Indoor Air* 2018; 28: 500–524.
15. Piirila P and Sovijarvi ARA. Objective assessment of cough. *Eur Respir J* 1995; 8: 1949–1956.
16. McCool FD. Global physiology and pathophysiology of cough: ACCP evidence-based clinical practice guidelines. *Am Coll Chest Phys* 2006; 129: 48S–53S.
17. Gupta JK, Lin CH and Chen Q. Flow dynamics and characterization of a cough. *Indoor Air* 2009; 19: 517–525.

18. Gao N and Niu J. Transient CFD simulation of the respiration process and inter-person exposure assessment. *Build Environ* 2005; 41: 1214–1222.
19. Wan MP, Chao CYH, Ng YD, To GNS and Yu WC. Dispersion of expiratory droplets in a general hospital ward with ceiling mixing type mechanical ventilation system. *Aerosol Sci Technol* 2007; 41: 244–258.
20. Tian ZF, Tu JY and Yeoh GH. CFD studies of indoor airflow and contaminant particle transportation. *Particul Sci Technol* 2007; 25: 555–570.
21. Deevy M, Sinai Y, Everitt P, Voigt L and Gobeau N. Modelling the effect of an occupant on displace displacement ventilation with computational fluid dynamics. *Energy Build* 2008; 40: 255–264.
22. Aliabadi AA, Rogak SN, Green SI and Barlett KH. CFD simulation of human coughs and sneezes: a study in droplet dispersion, heat and mass transfer. In: *Proceedings of ASME international mechanical engineering congress & exposition*, Vancouver, November 12–18 2010, ASME Paper IMECE2010-37331.
23. Yu HC, Mui KW, Wong LT and Chu HS. Ventilation of general hospital wards for mitigating infection risks of three kinds of viruses including Middle East respiratory syndrome coronavirus. *Indoor Built Environ* 2016; 26: 514–527.
24. Ding J, Yu CW and Cao SJ. HVAC system for environmental control to minimize the COVID-19 infection. *Indoor Built Environ* 2020; 29: 1195–1201.
25. Zhu S, Srebric J, Spengler JD and Demokritou P. An advanced numerical model for the assessment of airborne transmission of influenza in bus microenvironments. *Build Environ* 2012; 47: 67–75.
26. Zhang B, Guo G, Zhu C, JZ and Lin CH. Transport and trajectory of cough-induced bimodal aerosol in air-conditioned space. *Indoor and Built Environment*. Online First epub ahead of print, 22 July 2020; https://doi.org/10.1177/1420326X20941166
27. Zheng LJ, Chen QY, Xu J and Wu FL. Evaluation of intervention measures for respiratory disease transmission on cruise ships. *Indoor Built Environ* 2016; 25: 1267–1678.
28. Zhou Q, Qian H and Liu L. Numerical investigation of airborne infection in naturally ventilated hospital wards with central-corridor type. *Indoor Built Environ* 2016; 27: 59–69.
29. Feng ZB, Yu CW and Cao SJ. Fast prediction for indoor environment: models assessment. *Indoor Built Environ* 2019; 28: 727–730.
30. Rosti ME, Olivieri S, Cavaiola M, Seminara A and Mazzino A. Fluid dynamics of COVID−19 airborne infection suggests urgent data for a scientific design of social distancing. *Sci Rep* 2020; 10: 22426.
31. Cravero C and Satta A. A CFD model for real gas flows. In: *Proceedings of ASME turbo expo 2000: turbomachinery technical conference and exposition*, Munich, Germany, May 8–11 2000, ASME Paper 2000-GT-0518.
32. Cogliandro S, Cravero C, Marini M and Spoladore A. Simulation strategies for regenerative chambers in glass production plants with strategic exhaust gas recirculation system. In: 11th AIGE 2017, 2nd AIGE/IEETA Int. Conf., Genova, Italy, June 12–13 2017. *Int J Heat Technol* 2017; 35: S449–S445.
33. Cravero C, De Domenico D, Leutcha PJ and Marsano D. Strategies for the numerical modelling of regenerative pre-heating systems for recycled glass raw material. *Mmep* 2019; 6: 324–332.
34. Cademartori S, Cravero C, Marini M and Marsano D. CFD simulation of the slot jet impingement heat transfer process and application to a temperature control system for galvanizing line of metal band. *Appl Sci* 2021; 21: 1149.
35. Balachandar S, Zaleski S, Soldati A, Ahmadi G and Bourouiba L. Host-to-host airborne transmission as a multiphase flow problem for science-based social distance guideline. *Int J Multiphase Flow* 2020; 132: 103439.
36. Liu S and Novoselac A. Transport of airborne particles from an unobstructed cough jet. *Aerosol Sci Technol* 2014; 48: 1183–1194.
37. Bourouiba L, Dehandschoewercker E and Bush JWM. Violent expiratory events: on coughing and sneezing. *J Fluid Mech* 2014; 745: 537–563.
38. Schiller L and Naumann A. A drag coefficient correlation. *Zeitschrift des vereins deutscher ingenieure* 1935; 77: 318–320.
39. Launder BE and Spalding DB. The numerical computation of turbulent flows. *Comput Meth Appl Mech Eng* 1974; 3: 269–289.
40. Ranz WE and Marshall WR. Evaporation from drops. *Chem Eng Prog* 1952; 48: 141–146.
41. Zhao B, Zhang Z and Li X. Numerical study of the transport of droplets or particles generated by respiratory system indoors. *Build Environ* 2005; 40: 1032–1039.
42. ANSYS Inc. *Ansys CFX theory guide v 17*. Canonsburg, PA: ANSYS Inc., 2016.
43. Papinemi RS and Rosenthal FS. The size distribution of droplets in the exhaled breath of healthy human subjects. *J Aerosol Med* 1997; 10: 105–116.
44. Lin Z, Wang J, Yao T and Chow TT. Investigation into anti-airborne infection performance of stratum ventilation. *Build Environ* 2012; 54: 29–38.
45. Lin Z, Wang J, Yao T, Chow TT and Fong KF. Numerical comparison of dispersion of human exhaled droplets under different ventilation methods. *Wrstsd* 2013; 10: 142–161.
46. Mui KW, Wong LT, Wu CL and Lai ACK. Numerical modeling of exhaled droplet nuclei dispersion and mixing in indoor environments. *J Hazard Mater* 2009; 167: 736–744.
47. Yi H, Wang Q and Feng Y. Computational analysis of obstructive disease and cough intensity effects on the mucus transport and clearance in an idealized upper airway model using the volume of fluid method. *Phys Fluids* 2021; 33: 021903.
48. Mukhametzanov IT, Grinshpun SA, Zaripov SK and Gilfanov AK. Assessing the protection provided by face-piece filtering respirator: new model involving spherical porous layer with annular peripheral opening. *Aerosol Air Qual Res* 2016; 16: 2428–2437.

49. BS EN 14683:2014 (E). *Medical face masks. Requirements and test methods*. London: British Standards Institution, 2014.
50. Okubo T and Kobayashi H. Performance evaluation of masks for medical use - including the comparison with commercially available masks for general use. 医療関連感染 2008; 1: 57–61.
51. YouTube channel link of the "CFD Group" of the University of Genoa, www.youtube.com/channel/UCHa_j6PpCPJxBhcVAP1neRw (accessed 4 August 2021).